LA-UR-91-1525

Los Alamos National Laboratory is operated by the University of California for the United States Department of Energy under contract W-7405-ENG-36

TITLE: BEAM-DYNAMICS DESIGN AND PERFORMANCE OF THE RF DEFLECTOR IN THE LOS ALAMOS SINGLE-BEAM FUNNEL EXPERIMENT

AUTHOR(S): F. Guy, K. F. Johnson, and O. R. Sander

Los Alamos

Los Alamos National Laboratory
Los Alamos, New Mexico 87545

MASTER

FORM NO. 836 R4

Beam-Dynamics Design and Performance of the RF Deflector in the Los Alamos Single-Beam Funnel Experiment*

F. W. Guy,** K. F. Johnson, and O. R. Sander

Los Alamos National Laboratory, Los Alamos, NM 87545

Abstract

Funnels in which two bunched ion beams are interlaced to form a single beam have been proposed for high-current low-emittance ion linacs. A well-designed funnel would produce a beam with twice the frequency and current and almost twice the brightness of each original beam. A single-beam funnel experiment exploring the beam-dynamics and physics issues of a discrete-element funnel has been completed at Los Alamos National Laboratory (LANL). The only known beam-dynamics issue of concern in a two-beam funnel not addressed was the beam-beam interaction, which is negligible. The rf deflector, in which beam merging occurs, is a key component of a discrete-element funnel. We report the beam-dynamics design procedure and experimental results for the rf deflector.

I. INTRODUCTION

Low-emittance-growth funnel designs for low-beta, high-current ion beams can be divided into a transport, a merging, and a matching sections. The transport section matches the incoming beam to the funnel-focusing lattice, brings the beam to the proper position and angle, and provides the proper beam Courant-Snyder parameters for the merging section. The merging section interlaces the bunches to make a single beam. The matching section prepares the beam for the next accelerator. Charge-redistribution emittance growth [1] is controlled in the funnel by maintaining constant or smoothly varying focusing in the transverse and longitudinal directions.

The rf deflector is a key funnel element. At its input, bunches arrive off-axis and at an angle to the deflector centerline. The deflector bends them through a few degrees to exit along the centerline. Alternate bunches, from the two incoming beamlines, are deflected in opposite directions to form a single output beam. In the single-beam funnel this deflection was accomplished by an alternating electric field.

The Accelerator Test Stand (ATS) single-beam funnel experiment [2] consisted of a transport and merging section. The ATS 425-MHz, 5-MeV drift-tube linac (DTL) produced the H⁻ funnel input beam. Experimental objectives were to explore the beam-dynamics and physics issues of a low-emittance-growth funnel design and to validate computer code predictions. The only known beam-dynamics issue of concern in two beam funnels not addressed in the single-beam experiment was that of beam-beam interaction. In this type of design, beam-beam interaction occurs only in the merging section, and it has been shown [3] that the major effect is to deflect the beam at most a few tens of microradians.

The funnel beam-dynamics design was a joint effort of McDonnell-Douglas Corporation; AccSys, Inc.; and LANL [4]. The rf deflector design was by Walling et al. [5] at LANL.

II. BEAM-DYNAMICS CONSIDERATIONS

Consider a parallel-plate electric deflector of length d with a uniform time-dependent electric field $E_\perp = E_0 \cos(\omega t)$ perpendicular to the entering particle's path. We neglect end effects and the magnetic field. For small deflections the synchronous particle (which passes through the center of the deflector at t = 0) will be deflected through an angle [6]

$$x'(d) = \frac{2qE_0}{m_0\gamma c\beta\omega} \sin\left(\frac{\pi d}{\beta\lambda}\right) ,\tag{1}$$

where q and m_0 are the particle's charge and rest mass, $c\beta$ is its velocity, γ is the relativistic gamma, and $\lambda = 2\pi c/\omega$. Equation 1 shows that a x' maximum occurs when $d = \beta\lambda/2$. For a particle with phase σ relative to the synchronous particle, the deflection is (for $d = \beta\lambda/2$)

$$x'(\sigma) = \frac{2qE_0}{m_0\gamma c\beta\omega} \cos(\sigma) .\tag{2}$$

Equations 1 and 2 are approximate. They show some important points to be considered when designing a funnel rf deflector. Equation 1 gives an upper limit to the deflection for a given rf electric field and shows the mass, velocity, and frequency dependence. Equation 2 shows that, for a compact bunch (phase spread <1 radian), the difference in deflection between the synchronous particle and a particle of phase σ will be approximately proportional to σ^2 since $\cos(\sigma) = 1 - \sigma^2/2 + \sigma^4/4 - \ldots$ An rf deflector produces transverse emittance growth in a bunch partly because the head and tail will be deflected less than the center even if the bunch is phased for maximum deflection and minimum emittance growth. The shorter the bunch, the less transverse emittance growth. Thus the bunch should be compressed in the transport section, which may aid the longitudinal match into the next accelerator.

A real deflector will have a nonuniform electric field, particularly at the ends. End effects contribute to emittance growth; such growth occurs in all three planes and depends upon the configuration of the deflector and the bunch's configuration and trajectory. A detailed calculation must include the deflector and the rest of the funnel so that the bunch is correctly conditioned for entrance into the deflector. All important funnel parameters must be optimized together to minimize emittance growth. Optimization was an iterative procedure using various codes to calculate beamline electric fields from given deflector pole tip and aperture shapes; to transport bunches of particles through such fields for beam dynamics calculations; and to determine maximum rf peak surface electric fields, frequencies, and power requirements [5].

III. DESIGN METHODS

A funnel design starts with a layout based on geometrical considerations such as dimensions of the preceding accelerators

(e.g., RFQs), focusing periods, number of magnetic dipoles required, etc. TRACE calculations help determine focusing quadrupole and rebuncher strengths and component spacings. Equation 1 gives a limiting value to the deflection that can be achieved in the rf deflector. This value is combined with allowable pole-tip field strength and required focusing strength in the defocusing quadrupole(s) preceding the deflector to give approximate beam separation at the adjacent upstream focusing quadrupole. This quadrupole is the last element of the transport section. The maximum deflection angle is usually determined by peak surface field on deflector poles. Transverse emittance growth and maximum pole-tip field in the defocusing quadrupole can also limit the maximum angle. It is undesirable to push the deflection angle to the limit in normal operation. The ATS deflector was designed with a peak surface field of 1.7 Kilpatrick and a deflection angle of ~3.2°. It could reach higher deflection angles at higher power without sparking [5].

In a deflector design. the geometry of the poles and the entrance and exit apertures should be shaped for the highest beam-bend angle with the lowest peak surface field. Plots from CHARGE2D (a 2-D static electric field code) for the ATS design are shown in Fig. 1 (one quadrant of the pole and aperture nose configuration) and Fig. 2 (electric field along the surface of the pole). The pole-to-pole distance is specified to be the minimum necessary for comfortable beam clearance. Points of peak surface electric field will be where field lines converge on the surface (e.g., where the poles start to bend away from each other at the tips and where the pole tips are close to the entrance and exit aperture noses). Another high-field point can be off the beamline, where the aperture noses and the pole tips curve away from each other. The latter point does not show up on the 2-D calculation but must be considered in the 3-D rf design [5]. In the 2-D geometry we try to minimize and to keep equal the magnitudes of the surface electric field peaks. The goal is to maximize the region of relatively uniform electric field between the poles and to minimize the region of the nonlinear fringe field at the pole tips (that contributes to emittance growth). The peak surface field calculated by CHARGE2D for the ATS deflector pole tips was ~15% larger than in the middle of the poles. The pole tips have a constant radius in the bend plane; slight improvement in peak field might result from shaping the pole tips to produce a more uniform surface electric field.

A uniform-field deflector without end effects would have length βλ/2. A real deflector has end effects and it is not clear how long the poles should be for an optimum effective length. As a first approximation, we choose the "effective end" of the poles to be midway between the pole tips and the aperture noses. PARMILA calculations with the fields for this geometry allow one to find a value for pole rf voltage that gives the desired bunch deflection and value for emittance growth through the deflector. The deflector length is then changed slightly and its shape optimized to produce the lowest peak surface field and to equalize the two peaks' magnitudes. The resulting fields are then used in another PARMILA calculation. These iterations continue until a minimum voltage is found for the desired deflection angle. This procedure results in a curve of applied rf voltage vs deflector pole length for a given beam deflection angle and allows one to pick the proper pole length (usually corresponding to the minimum voltage). Emittance growth remains fairly constant

for small length changes, but there is a definite deflector length for minimum voltage.
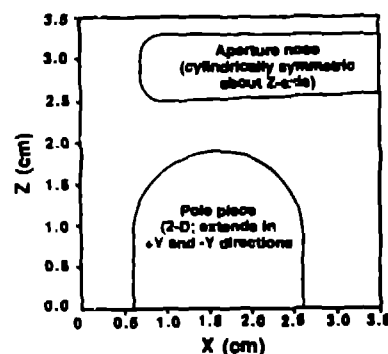

Figure 1. Cross section in the bend plane of one quadrant of deflector geometry from CHARGE2D.
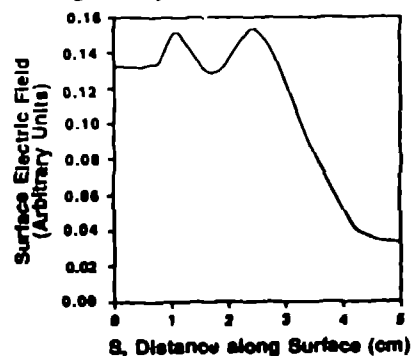

Figure 2. Surface electric field plot from CHARGE2D for pole geometry in Fig. 1.

The requirements of transverse focusing provide a constraint on deflector length. For minimum emittance growth we would like to gradually change the focusing lattice along the funnel from that of the preceding accelerator to that of the next one. Usually the next accelerator is a DTL with distance between centers of the first quadrupoles equal to βλ/2.

This leaves a drift gap considerably less than βλ/2 between the quadrupoles. The above procedure results in a deflector (with aperture noses) of more than βλ/2. A compromise is reached by placing the quadrupoles in the aperture noses (to reduce distance between the magnets along the deflector), by gradually extending the focusing lattice length in the transport section to allow room for the deflector, and by gradually decreasing the focusing length in the matching section to match into the next accelerator. The gradual increase and decrease in focusing length produces less charge-redistribution emittance growth than an abrupt change. For the ATS funnel the restriction on deflector length due to focusing length did not apply since there was no following accelerator. The focusing lattice was expanded to allow plenty of room for the deflector.

For funnel calculations, PARMILA has been modified by adding 3-D space charge (a point-to-point treatment) because of the 3-D nature of the space charge in the merging section. One version of PARMILA has a deflector subroutine that transports particles stepwise through a 2-D, time-dependent, electric field map generated by CHARGE2D. Another version uses a full 3-D map of static and time-dependent electric and magnetic fields in its deflector subroutine. The two PARMILA versions did not give significantly different results.

The 3-D fields are calculated by the MAFIA code, which was used in the cavity rf design and has the full 3-D geometry [5], and by PMELE, a permanent-magnet field code. In PARMILA these fields are overlapped so that in the deflector end regions the particles see the deflector rf electric and magnetic fields and the static magnetic fringe fields of the permanent-magnet quadrupoles. Other 3-D EM codes could be used to generate field maps. These modified PARMILA codes were used in the design of the ATS funnel and deflector. PARMILA does not take into account image charge forces resulting from conducting boundaries near the beamline. Image forces were included in a PARMILA-derived code for calculation of a heavy-ion RFQ funnel [7]; there image forces had little effect on emittance but did introduce some beam steering. Steering correctors are included in funnel designs (e.g., movable focusing quadrupoles).
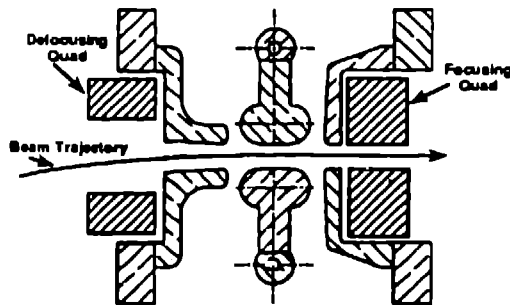

Figure 3. Cross section of deflector poles, noses, apertures, and magnets in plane of bend.

IV. EXPERIMENTAL PROCEDURES AND RESULTS

Figure 3 shows a cross-sectional sketch of the deflector in the bend plane close to the beamline. Funnel diagnostics included toroids to measure beam current and a movable diagnostic plate [2] (D-plate) on which were mounted transverse emittance measuring devices and beamline components for LINDA [8] (diagnostics for longitudinal beam parameters). The D-plate was installed to measure beam parameters at the entrance to the defocusing quads upstream of the deflect. After the deflector and associated quads were installed, the D-plate was placed downstream of the deflector to
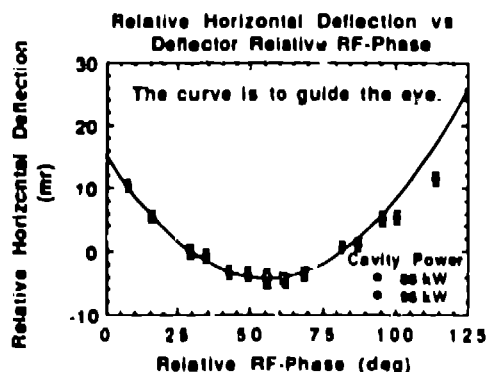

Figure 4. Deflection vs rf phase at design voltage.

measure its output beam. Beam trajectories were measured vs deflector rf phase (Fig. 4) and voltage (Fig. 5). Calculated and experimental trajectories agreed at the operating point of the deflector [2]. The measured emittance growth (in all planes)

was small, within experimental variations, and consistent with beam-dynamics code predictions [2]. No beam loss was detected through the deflector at nominal rf phase and voltage settings [2].
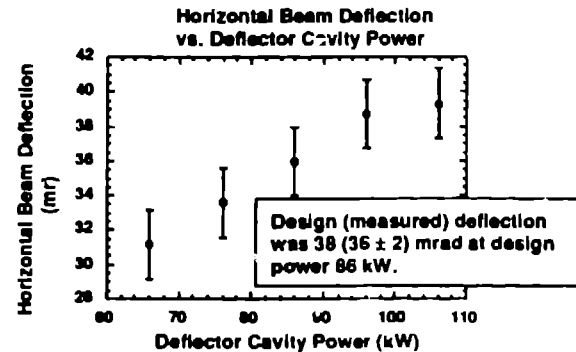

Figure 5. Deflection vs cavity power.

V. SUMMARY AND CONCLUSIONS

An rf deflector design for a funnel line requires attention to details. The whole beamline, including the preceding and following accelerators, must be taken into account. Attention must be paid to the configuration of the deflector elements and to the conditioning of the beam prior to entrance into the deflector. The ATS single-beam funnel experiment showed that, with present methods and techniques, one can produce funnel and deflector designs with very low emittance growth.

The ATS rf deflector was successful. Calculations and experimental results agreed within experimental errors, showing that rf and beam-dynamics design procedures were correct and that no important physics was omitted in the codes.

VI. REFERENCES

[1] T. P. Wangler, et al., "Emittance Growth from Charge Density Changes in High-Current Beams," Proc. Intl. Symp. on Heavy Ion Fusion, Washington, DC, 1986, p. 156.

[2] K. F. Johnson, et al., "The Single-Beam Funnel Demonstration: Experiment and Simulation," Proc. 1990 Linear Accelerator Conference, LANL report LA-12004-C (March 1991) p. 701; "A Beam Funneling Demonstration: Experiment and Simulation," Particle Accelerators (1991).

[3] F. W. Guy, "Beam-Beam Interaction in High-Current Ion Funnels," LANL memo AT-1:90-104, March 19, 1990.

[4] R. J. Kashuba, et al., "The Magnetic Optics Design of the ATS Funnelling Experiment," LANL report LA-CP-89-277 (1989).

[5] L. S. Walling, et al., "Design and Test Results of a Robust, High-Field RF Deflector for Beam Funnelling," LANL report LA-CP-90-201 (1990).

[6] K. Bongardt and D. Sanitz, "Funnelling of Heavy Ion Beams," Proc. Symp. Accelerator Aspects of Heavy Ion Fusion, Gesellschaft für Schwerionenforschung report GSI-82-8 (1982), p. 224.

[7] F. W. Guy and R. !! Stokes, "Simulation of an RFQ Funnel for Heavy Ion Beams," Proc. 1989 IEEE Particle Accelerator Conference, Chicago, IL, 1989, 833.

[8] W. B. Cottingame, et al., "Noninterceptive Technique for the Measurement of Longitudinal Parameter of Intense H Beams," Proc. 1985 Particle Accelerator Conference, IEEE Trans. Nucl. Sci. 32(5) 1985, p. 1871.